

Continuously observing the spectrum of a dynamically decoupled spin-1 quantum gas

R. P. Anderson,¹ M. J. Kewming,¹ and L. D. Turner¹

¹*School of Physics & Astronomy, Monash University, Victoria 3800, Australia.*

(Dated: June 14, 2017)

Quantum states and spectra can be made sensitive to a particular measurand whilst simultaneously impervious to parasitic fluctuations of an environment. Here we use an atom-light interface with minimal backaction to probe the spectrum of a radiofrequency-dressed spin-1 quantum gas continuously and in-situ. The dressing amplitude sets the radiofrequency band in which oscillating magnetic fields manifest a linear measurand, and we probe the energy spectrum and coupling strengths during unitary evolution of the system. By varying a symmetry-breaking parameter of the Hamiltonian, we find a regime in which two of the dressed states are maximally insensitive (up to fourth-order) in magnetic field fluctuations that are slow compared to the dressed-state splittings. Moreover, we demonstrate the predictive power of our continuous probe to optimize the dynamical decoupling and tune the measurement band. This robust system shares the useful hallmarks of quantum metrology platforms; the states are thus termed “synthetic clock” states in a complementary result by Lundblad et al. (arXiv:1706.xxxx) and are candidates for band-tunable magnetometry and emulation of quantum magnetism in solid-state systems.

From Hahn echoes to contemporary dynamical decoupling, abrupt, discrete rotations have been used to protect spin superpositions from inhomogeneities and parasitic fluctuations, prolonging quantum coherence and circumventing deleterious energy shifts [1–3]. A complementary strategy is to replace the pulse train with an uninterrupted coupling of ‘bare’ spin states, thus admitting new ‘dressed’ spin eigenstates, with a modified quantization direction, spectrum, and coupling, which too are protected from unwanted artifacts of their environment [4]. This *continuous* dynamical decoupling (CoDD) has proven useful across multiple platforms including nitrogen-vacancy centers [5–8] and superconducting qubits, and forms the basis for creating protected qubit [9] and decoherence-free [10] subspaces. Weak continuous measurement is a powerful instrument for appraising and refining dynamical decoupling in real time; to probe stochastic evolution, improve metrological bandwidth, or realize quantum feedback schemes [11]. Here we use dispersive optical readout of a ‘bare’ spin component \hat{F}_x to measure the spectrum of a continuously decoupled spin-1 quantum gas using time-resolved Fourier spectroscopy. Fourier transform spectroscopy has been to measure band structures of a spin-orbit coupled BEC [12] by composing multiple non-contiguous projective measurements. The rich time-frequency domain data in our experiment reveal not only multiple dressed-state splittings and their relative immunity to noise, but also dressed state coherences and coupling strengths. This potent ability to estimate the eigenspectrum of a multi-level dressed system reveals features absent in spin-1/2 or composite spin-1/2 qubit systems; principally, we identify a regime in which a subspace of the dressed system is maximally decoupled from noise $\propto \hat{F}_z$. This subspace is spanned by two of the dressed states, termed ‘synthetic clock states’ in a co-submission by Lundblad et al. (arXiv:1706.xxxx). The low-frequency magnetic stabil-

ity and high-bandwidth detection of these states is immediately applicable to band-tunable (ac) magnetometry [5, 6, 13] and experiments preparing delicate spin-entangled many-body states [14]; whereas the unconventional cyclic coupling of all $2F + 1$ dressed states could be applied to emulation of frustrated quantum spin chains [15].

Atomic Zeeman states $|m_z = -1, 0, 1\rangle$ in a magnetic field $B_z \mathbf{e}_z$ can be decoupled from fluctuations in B_z by applying a perpendicular radiofrequency (rf) field ~~perpendicular to the quantization direction z , of amplitude $B_{\text{rf}} \mathbf{e}_x$, and oscillating $B_{\text{rf}} \mathbf{e}_x \cos \omega_{\text{rf}} t$, oscillating at ω_{rf} , tuned near the splitting of the ‘bare’ Zeeman states Larmor frequency $\omega_L \equiv (E_{m_z=+1} - E_{m_z=-1})/2\hbar$, the Larmor frequency~~. At low magnetic fields, the degeneracy of the composite spin-1/2 systems [16] renders the spin-1 behavior identical to CoDD in spin-1/2 qubits. ~~The systems. In the dressed-state picture, the spin is quantized along x in a frame rotating with the radiofrequency ω_{rf} , i.e. the eigenstates of $\mathcal{H}_{\text{rwa}} = \Delta \hat{F}_z + \Omega \hat{F}_x$ are $|m_x = -1, 0, 1\rangle$, with energies $m_x \hbar \sqrt{\Omega^2 + \Delta^2}$, where $\Delta = \omega_{\text{rf}} - \omega_L$ is the detuning and $\Omega = \gamma B_{\text{rf}}/2$ is the Rabi frequency. The rf dressing reduces the Radiofrequency dressing induces an avoided crossing in the dressed energy spectrum, at resonance $\Delta = 0$ reducing the leading-order linear sensitivity of the ‘bare’ state energies ($\omega_L \approx \gamma B_z$ where γ is the gyromagnetic ratio) to magnetic field variations δB_z to quadratic sensitivity, via the detuning Δ , from linear to merely quadratic sensitivity.~~ The spin character and symmetries are otherwise unchanged; ~~magnetic fields along y or z ; transverse magnetic fields~~ oscillating near the ~~Rabi frequency splitting frequencies drive transitions between eigenstates. In the dressed system this means relatively low-frequency (‘ac’) fields oscillating near the Rabi frequency Ω , such as $B_{y,\text{ac}} \mathbf{e}_y \cos \Omega t$ and $B_{z,\text{ac}} \mathbf{e}_z \cos \Omega t$, drive transitions $|m_x = -1\rangle \leftrightarrow |m_x = 0\rangle$ and $|m_x =$~~



FIG. 1. Energy spectrum and splittings of a radiofrequency coupled spin-1 for various $q \in [0, \Omega]$. The transparency of each curve is proportional to the distance of q/Ω from $q_{R,\text{magic}}$ in Eq. (1). (Left) Energies ω_n of dressed states $|n\rangle = |1\rangle$, (red) $|2\rangle$ (blue), and $|3\rangle$ (green) normalized to the rf-coupling strength (Rabi frequency) Ω as a function of detuning $\Delta = \omega_{\text{rf}} - \omega_L$. Dashed lines indicate the energies of uncoupled states ($\Omega = 0$) in a frame rotating at ω_{rf} . (Right) Splittings ω_{ij} of dressed states $|i\rangle$ and $|j\rangle$ as a function of detuning. When $q/\Omega = q_{R,\text{magic}}$ (bold curves), energies ω_1 and ω_2 share the same curvature, and their difference ω_{12} (right, purple) is minimally sensitive to detuning and thus magnetic field variations.

$0\rangle \leftrightarrow |m_x = +1\rangle$. This is the basis for ac magnetometry [5] or concatenated CoDD to mitigate of relatively low-frequency fields; and for concatenated CoDD which protects against fluctuations in Ω on the spectrum and coherences [7]. Insensitivity to wider bandwidth and larger amplitude δB_z can be achieved by increasing Ω , opening a broader gap in the dressed spectrum, but doing so changes the bandwidth of the exquisitely sensitive quantum lock-in detection recently demonstrated using NV centers [17]. Henceforth we presume Ω is fixed by the signal of interest application.

However, any \hat{F}_z^2 interaction – arising from non-linear Zeeman [18], microwave ac-Stark [19], or tensor light [20] shifts – raises the degeneracy of the $|m_z = -1\rangle \leftrightarrow |m_z = 0\rangle$ and $|m_z = 0\rangle \leftrightarrow |m_z = +1\rangle$ transitions, and breaks the symmetry of $\mathcal{H}_{\text{rwa}} = \Delta \hat{F}_z + \Omega \hat{F}_x + q \hat{F}_z^2$, where $q \equiv (E_{m_z=+1} + E_{m_z=-1} - 2E_{m_z=0})_{\Omega=0}/2\hbar$. This yields dressed eigenstates $\{|1\rangle, |2\rangle, |3\rangle\}$ that are no longer SO(3) rotations of the bare Zeeman states $|m_z\rangle$, but have nematic order [LDT: $|m_z = 0\rangle$ is nematic!], and an eigenspectrum $\omega_i(\Delta) = E_{|i\rangle}/\hbar$ shown in Fig. 1 (left) for $q \in [0, \Omega]$. Moreover, the coupling of couplings between these dressed states is are markedly different: the spin operators $\hat{F}_{x,y,z}$ [Susbscript for dressed operators?] in the dressed basis span more of SU(3) for $q \neq 0$, e.g. The matrix element $\langle i | \hat{F}_x | j \rangle$ has a non-zero projection onto the Gell-Mann matrix λ_4 signifying the for all i, j signifying direct coupling of dressed states

$|1\rangle$ and $|3\rangle$. The dressed-state transitions are thus cyclic and non-degenerate (right), characterized by, in contrast to the bare states where only adjacent states are coupled. Just as for bare states, we can characterize the splittings [we are using splittings and transitions around here...] between dressed states near $\Delta = 0$ as arising from a dressed Larmor frequency

$$\omega_D \equiv (\omega_3 - \omega_2)_{\Delta=0}/2 = (\omega_{12} + \omega_{23})_{\Delta=0}/2 = \sqrt{\Omega^2 + q_D^2},$$

$\omega_D \equiv (\omega_3 - \omega_1)/2 = \sqrt{\Omega^2 + q_D^2}$, and dressed quadratic shift

$$q_D \equiv (\omega_3 + \omega_1 - 2\omega_2)_{\Delta=0}/2 = (\omega_{23} - \omega_{12})_{\Delta=0}/2 = -q/2.$$

The $q_D \equiv (\omega_3 + \omega_1 - 2\omega_2)/2 = -q/2$, giving splittings $\omega_{23} = \omega_D - q_D$, $\omega_{12} = \omega_D + q_D$ and $\omega_{13} = 2\omega_D$.

A figure-of-merit for decoupling is the curvature of the dressed state energies $\omega_i(\Delta)$ depends on transition frequency at resonance. In a dressed two-level system there is one convex and one concave eigenstate and splitting is simply convex. Figure 1 shows that in our three-level system with quadratic shift, two states are convex. At a particular value of the normalized quadratic shift $q_R = q/\Omega$, and $q_R = q/\Omega$ the curvature is equal for states $|1\rangle$ and $|2\rangle$ when and the curvature of ω_{12} vanishes. This ‘magic’ value is [21]

$$q_R = q_{R,\text{magic}} = \sqrt{(3\sqrt{2} - 4)/2} \approx 0.348. \quad (1)$$

resulting in vanishing quadratic dependence of their transition frequency $\omega_{12} = \omega_2 - \omega_1$ on Δ [22]. The leading-order sensitivity of these states to field variations δB_z at $q_{R,\text{magic}}$ is quartic [23], amounting to their optimal CoDD and we join in giving the subspace comprised of $|1\rangle, |2\rangle$ a higher-order decoupling than can be achieved with a two-level system; [... or similar bombastic sentence. This needs oomph.] [Need to decide on spin-1/2 versus two-level etc.] we join Lundblad et al. in terming them these ‘synthetic clock states in this configuration’.

We experimentally demonstrate this optimal CoDD using—

We optimise of this high-order decoupling in the laboratory with a continuous measurement of the dressed spectrum of a spin-1 non-degenerate quantum gas. Using a single realisation of the quantum gas, we adiabatically increase the detuning from resonance making many successive measurements, each of which simultaneously measures all three splittings ω_{ij} between the dressed states. Our spinor quantum gas apparatus [24] and

Faraday atom-light interface are described in greater detail elsewhere [25]. We prepare an ultracold gas ($\sim 1 \mu\text{K}$) of approximately 10^6 ^{87}Rb atoms in a crossed-beam optical dipole trap ($\lambda = 1064 \text{ nm}$). A radiofrequency field of amplitude $\Omega/(2\pi) < 100 \text{ kHz}$ couples the three Zeeman states $|m_z = -1, 0, +1\rangle$ of the lowest hyperfine ($F=1$) ground state coupled using a radiofrequency field with $\Omega/(2\pi) \leq 100 \text{ kHz}$, generated by a single-turn coil placed immediately atop the glass vacuum cell, fed by an amplified radiofrequency source generated using direct-digital synthesis. A component of the collective spin ground state. To perform a weak measurement of the evolving spin, we focus a linearly polarized far-off-resonant probe beam ($\lambda = 781 \text{ nm}$) onto the atoms. The spin component Larmor precession transverse to the static magnetic field direction (along z) constant magnetic bias field rotates the polarization of an off-resonant probe beam the probe via the paramagnetic Faraday effect; shot-noise limited polarimetry of the optical probe in a bandwidth near the Larmor frequency ω_L thus measures reveals $\langle \hat{F}_x \rangle$.

Weak continuous measurement as an modulated tone near ω_{rf} . Similar weak continuous measurements using the paramagnetic Faraday effect has have been used to observe spin-mixing dynamics of a polar spinor condensate [26] and perform quantum state tomography [20, 26]. Similar polarimetry-based dispersive probes have been used to measured hyperfine Rabi oscillations of the collective clock-transition pseudospin [27]; modulating the birefringence of the atomic ensemble near baseband, resulting in polarization rotation oscillating at the Rabi frequency.

To probe the dressed state spectrum and coherences, we prepare a superposition of dressed states by abruptly suddenly turning on the Rabi coupling Ω at $t = 0$, projecting the polarized collective spin $|m_z = -1\rangle$ onto $|\psi(t=0)\rangle = \sum_i c_i |i\rangle$. The total magnetic field in the laboratory frame used to affect this control is $\mathbf{B}(t \geq 0) = -B_{\text{rf}} \cos(\omega_{\text{rf}} t) \mathbf{e}_x + B_z(t) \mathbf{e}_z$, where $B_z(t)$ varies slowly compared to Ω . The resulting Faraday signal is presented in the time-frequency domain using the short-time Fourier transform (spectrogram), revealing the rich frequency and amplitude modulation related to the dressed state energies, coherences, and coupling strengths. For example, with no deliberate variation of the Rabi frequency or detuning, we observe the spectrogram amplitude shown in Fig. 2. Strong amplitude modulation of the Faraday signal is apparent from the three upper and lower sidebands, each pair equidistant from the carrier frequency at $f_{\text{rf}} = \omega_{\text{rf}}/(2\pi)$. Each pair of sidebands corresponds to a dressed state transition $|i\rangle \leftrightarrow |j\rangle$; centered at with sideband frequencies $f_{\text{rf}} \pm f_{ij}$ where $f_{ij} = \omega_{ij}/(2\pi)$; the frequency of the transition. In this way, the spectrogram is a calibration-free, real-time measurement of the dressed state spectrum. Restricting attention to

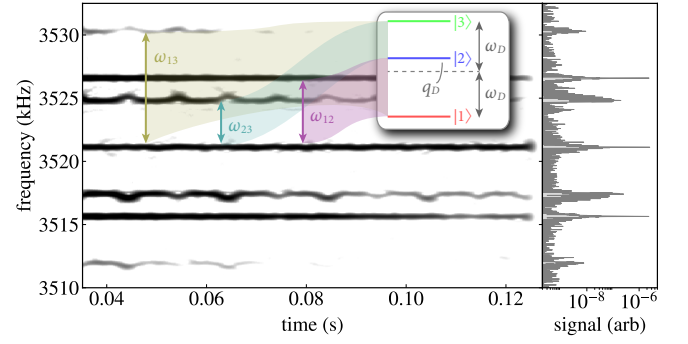


FIG. 2. Continuous measurement of the dressed energy spectrum for $q_R = 0.402(3)$, $f_{\text{rf}} = 3.521 \text{ MHz}$ and $B_0 = 5.013 \text{ G}$ (left) and a periodogram of the 100 ms long signal (right). (Inset) The dressed state energy diagram for resonant coupling ($|\Delta| \ll \Omega$); the mean and difference of transition frequencies ω_{12} and ω_{23} is the dressed Larmor frequency ω_D and quadratic shift q_D , respectively. The upper sidebands about the carrier at f_{rf} are associated with the ω_{13} (gold), ω_{23} (turquoise), and ω_{12} (lavender) transitions. Magnetic field fluctuations $\delta B_z = \delta B_{\text{ac}}(t)$ of amplitude 1.4 mG induced by mains power are manifest as asymmetric frequency modulation of the ω_{13} and ω_{23} sidebands, while the ω_{12} transition remains relatively unaffected. The corresponding spectral peaks have linewidths 102 Hz, 97 Hz, and 24 Hz, respectively. The ω_{12} linewidth is transform-limited, whereas the broadened peaks of the less decoupled ω_{23} transition exhibit a skew (third-moment) of 84 Hz (upper sideband) and -100 Hz (lower sideband).

the upper sidebands, the two closest to the carrier are ladder-type adjacent state transitions ω_{12} and ω_{23} have with similar amplitudes and lifetimes, with frequency separations $\omega_D \pm q_D$ from the carrier, respectively, for near-resonant coupling of the bare Zeeman states ($|\Delta| \ll \Omega$). The third, weaker sideband near $2\omega_D$ above the carrier is a signature of signifies the cyclic $|1\rangle \leftrightarrow |3\rangle$ transition, permitted only appearing when $q \neq 0$. No attempt was made to shield the apparatus from parasitic magnetic fields, and mains power induced. Power line magnetic field noise causes a temporally varying $\delta B_z = \delta B_{\text{ac}}(t)$ $\delta B_z \approx \delta B_{\text{line}}(t)$ at the line frequency of 50 Hz and its odd harmonics, of peak-to-peak amplitude $\sim 1.4 \text{ mG}$ (1 kHz in frequency units of detuning) peak-to-peak. For these data $q_R = 0.402(3)$, and each dressed transition is affected by the magnetic fluctuations differently; the sidebands corresponding to the ω_{13} and ω_{23} transitions exhibit asymmetric frequency modulation, whereas the optimally decoupled ω_{12} transition remains relatively unaffected. This is signified by skewed peaks in the unperturbed within the frequency resolution of this spectrogram. A periodogram (Fig. 2, right) of the entire time-series yields maximum frequency resolution (at the expense of all temporal resolution) shows the outwardly-skewed peaks expected for transitions convex in Δ , e.g. the ω_{23} sidebands have a third-moment of 84 Hz (upper) and -100 Hz (lower), and a linewidth

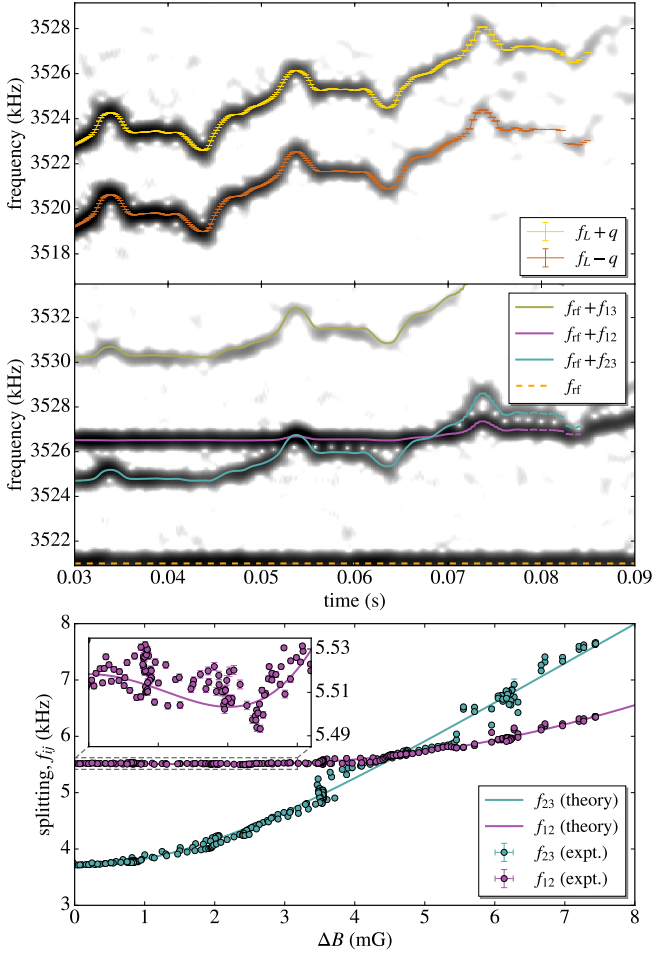


FIG. 3. Real-time CoDD observation for $q_R = 0.402(3)$. (a) and (b) are spectrograms of a continuous weak measurement of $\langle \hat{F}_x \rangle$. (a) Magnetometry of the bare Zeeman states ($\Omega = 0$) used to calibrate $B_z(t) = B_0 + \delta B_z(t)$ over the interrogation interval, in which the field [detuning] varies over a range $\sim B_{rf}$ [2Ω]. We numerically track the bare Zeeman splittings (gold/orange) to determine the instantaneous Larmor frequency $f_L(t)$ and quadratic shift $q(t)$. (b) The field is swept over the same range but the rf dressing is applied ($\Omega > 0$). Three sidebands above (shown) and below the carrier at $f_{rf} = 3.521$ MHz (dashed, orange) reveal the dressed state splittings $f_{ij} = \omega_{ij}/(2\pi)$. (c) A parametric plot of $f_{12}(t)$ and $f_{23}(t)$ versus $\delta B_z(t)$ by combining analysis of (a) and (b). Solid curves in (b) and (c) are theoretical splittings from an eigenspectrum calculation, provided only f_{rf} , $B_z(t)$, and Ω , i.e. no free parameters. Variation of the synthetic clock transition f_{12} for $0 \leq \delta B_z \leq B_{rf}/4 = 3.2$ mG (c, inset).

substantial third moments [Are we sure units of third moments are Hz not Hz³?] and a second moment (standard deviation) that is 4 times broader than the transform-limited [no, transform limited should be a few Hz only!] peak of the ω_{12} transition (24 Hz second-moment).

The amplitude of each sideband is proportional to the corresponding dressed-state coherence $e_i^* e_j = \rho_{ij}$, and $\rho_{ji} = c_i^* c_j$, and to the dressed state coupling

strength induced by the relevant spin projection operator $\hat{F}_{x,y,z}$ [Which is relevant to us? How do I know?]. For near-resonant coupling of the bare Zeeman states, an analytic expression for the amplitudes can be obtained, coupling amplitudes near resonance ($\Delta \ll \Omega$) is summarized in Table I. These depend on the initial projection onto the dressed basis, which if known permits amounts to continuous measurement of all coupling strengths in the dressed basis, an analogue of effecting Hamiltonian parameter estimation. Alternatively, independent characterization of the dressed-system couplings [process tomography/ Hamiltonian learning]. Alternatively, if the dressed state couplings [28] permits are separately characterized [28], this amounts to real-time measurement of the dressed density matrix, an analogue of effecting quantum state estimation. Metrics of the dressed system [I don't like 'amounts to'], metrics for the fidelity of dynamical decoupling vary amongst platforms, and in addition to linewidth narrowing include prolonged coherence. We nominally observe a three-fold increase in the lifetime of the spectral components corresponding to the ω_{12} and ω_{23} transitions as compared with the undressed system (Fig. 3a, $1/e$ decay time 23.8(2) ms). The dressed-state coherences are expected to be greater, but were limited here to ~ 100 ms by probe-induced photon scattering; admitting a lower signal-to-noise ratio using less perturbative probe [25] would permit even longer coherences to be revealed.

To appraise the relative CoDD of o appraise the success of decoupling of the dressed state transitions, and their dependence on the quadratic shift q_R , we varied the magnetic field over a wider range than in was furnished by our power line noise of Fig. 2, by sweeping the bias magnetic field along z over a range B_{rf} [What is this B_{rf} ?] during the measurement interval. [We should tread lightly here on this previous comment. We should avoid drawing attention to the question "If it is optimally decoupled, then it should show the longest de-coherence time. Have you done this?"] The control field $B_z(t) = B_0 + \alpha t + B_{ac}(t)$ $B_z(t) = B_0 + \alpha t + B_{line}(t)$, where $\alpha = 128$ mG/s is the linear sweep rate; the resulting detuning variation is of order 2Ω (cf. the domain of Fig. 1). For each realization (or 'shot') of the experiment, we directly calibrate $B_z(t)$ using magnetometry of the bare Zeeman states; an rf $\pi/2$ -pulse (rather than continuous coupling) initiates Larmor precession of the collective spin in the x - y plane, and the Faraday signal is composed of two tones at $\omega_{\pm} = \omega_L \pm q$, the bare Zeeman splittings (Fig. 3, top). For $q\tau_f \geq 2\pi$, where τ_f is the length of the overlapping spectrogram windows spectrogram window, the two tones are spectrally resolved and their mean and difference yields the instantaneous $\omega_L(t)$ and $q(t)$, the former of which is respectively, ω_L is then used to find $\delta B_z(t)$ (and $\Delta(t)$) by inverting the Breit-Rabi equation [18] [29].

We measured the dressed spectrum for a range of

TABLE I. Upper sidebands of the carrier (at ω_{rf}) of the Faraday rotation signal $\propto \langle \hat{F}_x \rangle$ of an arbitrary dressed state superposition driven on resonance ($\Delta = 0$). Frequency and phase are reported relative to the carrier, along with the transition that each sideband corresponds to. For the initial state $|\psi(t=0)\rangle = |m_z = -1\rangle$, the sideband frequencies and amplitudes can be concisely expressed in terms of the dressed Larmor frequency ω_D and quadratic shift q_D . For each upper sideband, there is a lower sideband of the same amplitude, relative frequency and opposite relative phase. [Note removal of curls and fracbracks in cols 4 and 5 resp of table to reduce symbology. Debatable!]

transition	frequency	$\omega_{ij} - \omega_{\text{rf}}$ ($\Delta = 0$)	amplitude ($\Delta = 0$)	amplitude
(carrier)	ω_{rf}	0	$(\langle 3 \hat{F}_x 3\rangle - \langle 1 \hat{F}_x 1\rangle)(\rho_{33} - \rho_{11})$	
$ 1\rangle \leftrightarrow 2\rangle$	$\omega_{\text{rf}} + \omega_{12} \omega_{\text{rf}} \pm \omega_{12}$	$\omega_D + q_D$	$-2i\langle 1 \hat{F}_y 2\rangle \text{Re}\{\rho_{12}\} = -2\langle 2 \hat{F}_z 3\rangle \text{Re}\{\rho_{12}\} - 2i\langle 1 \hat{F}_y 2\rangle \text{Re}\rho_{12} = -2\langle 2 \hat{F}_z 3\rangle \text{Re}\rho_{12}$	q_D
$ 2\rangle \leftrightarrow 3\rangle$	$\omega_{\text{rf}} + \omega_{23} \omega_{\text{rf}} \pm \omega_{23}$	$\omega_D - q_D$	$2i\langle 2 \hat{F}_y 3\rangle \text{Re}\{\rho_{23}\} = 2\langle 1 \hat{F}_z 2\rangle \text{Re}\{\rho_{23}\} - 2i\langle 2 \hat{F}_y 3\rangle \text{Re}\rho_{23} = 2\langle 1 \hat{F}_z 2\rangle \text{Re}\rho_{23}$	
$ 1\rangle \leftrightarrow 3\rangle$	$\omega_{\text{rf}} + \omega_{13} \omega_{\text{rf}} \pm \omega_{13}$	$2\omega_D$	$2\langle 1 \hat{F}_x 3\rangle \text{Re}\{\rho_{13}\} - 2\langle 1 \hat{F}_x 3\rangle \text{Re}\rho_{13}$	q_D

resonant magnetic fields $B_0 \in [3.549, 5.568] \text{ G}$ magnetic bias fields B_0 ranging from 3.549 to 5.568 G (applied rf frequency $f_{\text{rf}} \in [2.493, 3.911] \text{ MHz}$ frequencies f_{rf} from 2.493 to 3.911 MHz), with a fixed Rabi frequency of $\Omega/(2\pi) = 4.505(3) \text{ kHz}$ ($B_{\text{rf}} = 12.83(1) \text{ mG}$). For each resonant $\Omega = 2\pi \times 4.505(3) \text{ kHz}$. At each field B_0 , we ensured the Rabi frequency was fixed by measuring the voltage drop across the coil at f_{rf} with an rf lock-in amplifier which – in concert with an impedance analyzer – could be used to ensure the rf current in the coil and thus B_{rf} and Ω were constant. The Rabi frequency was ultimately measured using the atoms by analyzing a subset of the dressed energy spectrum during the magnetic field sweep when $|\Delta|/(2\pi) \leq 100 \text{ Hz}$ $\Delta \leq 2\pi \times 100 \text{ Hz}$ [no need for $|\cdot|$ as we always swept up, right?]. The measured Rabi frequencies had a standard deviation $\sigma(\Omega) = 9.4 \text{ Hz}$, validating the above method.

The dressed spectrum for the swept control field with resonant field $B_0 = 5.013 \text{ G}$ and $q_R = 0.403(2)$ is shown in Fig. 3b. The instantaneous dressed state splittings for all three transitions were predicted with no free parameters, and are plotted atop the spectrogram data, showing excellent agreement with the measured sidebands. Because $\delta B_z(t)$ is non-linear and non-monotonic in time, we use the raw time series from the calibration ($\Omega = 0$) and CoDD shots to form parametric ($\delta B_z(t)$, $f_{ij}(t)$) data, by tracking the instantaneous peaks in each spectrogram. The sensitivity of the $|1\rangle \leftrightarrow |2\rangle$ and $|2\rangle \leftrightarrow |3\rangle$ transitions to magnetic field variations are shown in Fig. 3c. The synthetic clock transition is most insensitive; the measured [predicted] f_{12} varies by 39 Hz [26 Hz] for $0 \leq \delta B_z \leq B_{\text{rf}}/4 = 3.2 \text{ mG}$ (Fig. 3c, inset). The corresponding normalized variation in $\omega_{12}/\Omega = 8.6 \times 10^{-3}$ [5.8×10^{-3}] across a detuning range of $0 \leq |\Delta/\Omega| \leq 0.5$. By comparison, the normalized variation at $q_R = 0$ is $(\sqrt{5} - 2)/2 \approx 0.118$; 14 [20] times higher than the observed [predicted] variation. Alternatively, the normalized variation of the $|m_z = \pm 1\rangle \leftrightarrow |m_z = 0\rangle$ Zeeman transitions at $q = 0$ is 0.5; 58 [86] times higher than the observed [predicted] variation in the synthetic clock

transition frequency.

In the adiabatic limit, the dressed state populations remain constant and the above superposition evolves under phase acquisition $e^{-i\omega_i t}$ by each dressed state $|i\rangle$ [30]. We quantify the stasis of the dressed superposition using the generalized adiabatic parameter $\Gamma \equiv |\Omega(t)/\dot{\theta}(t)|$, where $\Omega = \mathbf{B}_{\text{eff}}/\gamma \equiv \Omega \mathbf{e}_x + \Delta \mathbf{e}_x$ and $\tan \theta \equiv \Omega/\Delta$. [If using Γ must say that $\Gamma \gg 1$ means adiabatic or whatever...] For constant coupling amplitude $\dot{\Omega} = 0$, $\dot{\theta}(t) = -\Omega\Delta(t)/|\Omega|^2$. For the magnetic field sweeps used here, $\Gamma > 200$ and $\sqrt{\langle \Gamma^2 \rangle}_t \gtrsim 600$ where $\langle \cdot \rangle_t$ denotes the time-average over the duration of the sweep Γ exceeded 200 everywhere and was on average > 600 . Nevertheless, the continuous spectra when plotted parametrically (Fig. 3c) exhibit some evidence of non-adiabatic following. This is corroborated by numerically integrating [do they?] Numerical integration of the Schrödinger equation of the known control Hamiltonian; the confirms that dressed state populations vary slowly (compared to ω_D^{-1}) but by a few percent near minima of $\Gamma(t)$, i.e. when the sweep is least adiabatic. deviate by no more than X% from their initial values.

To test the predictive power of our CoDD measurement, we inferred measurement of dynamical decoupling, we determined the curvature of the synthetic clock transition with respect to magnetic field variations, inspecting the quadratic coefficient of a polynomial fit to $(\delta B_z, f_{12})$ data. The results of this model independent analysis are shown in Fig. 4 for $q_R \in [0.2, 0.5]$ q_R between 0.2 and 0.5. The curvature $\partial^2 f_{12}/\partial B_z^2$ can be predicted analytically, and varies near-linearly is predicted analytically to be near-linear in q_R over this range. Accordingly, we perform linear regression to the measured curvature versus q_R to infer $q_{R,\text{magic}}$, where the synthetic clock transition has vanishing curvature, and find $q_{R,\text{magic}}$ (expt.) = 0.350(6), in agreement with the theoretical value in Eq. (1). The minimum curvature demonstrated here occurs measured occurred at $q_R = 0.351(2)$, with a value of $(\partial^2 f_{12}/\partial B_z^2)_{\text{min}} = 10^{-3} \text{ kHz/mG}^2$ $(\partial^2 f_{12}/\partial B_z^2)_{\text{min}} = 1 \text{ Hz/mG}^2$ [1 MHz/G²]. In dimen-

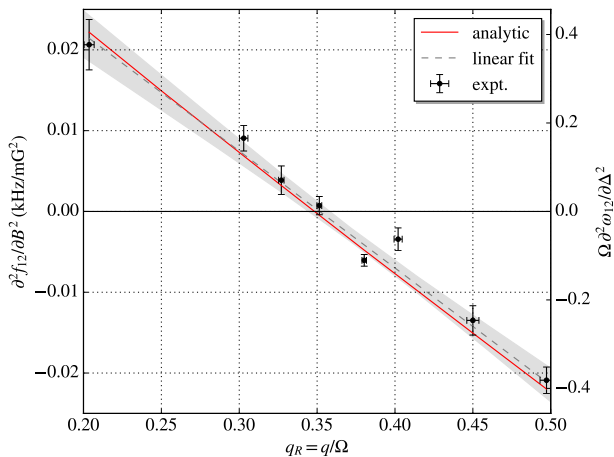


FIG. 4. Curvature of the synthetic clock transition for normalized quadratic shifts $q_R \in [0.2, 0.5]$. The measured curvature (black points) was determined from polynomial fitting to $(\delta B_z, f_{12})$ data shown in Fig. 3(c). Vertical and horizontal error bars correspond to the standard error of the regression and uncertainty in q_R (via $u(q)$ and $u(\Omega)$ at each field B_0), respectively. A linear fit (black, dashed) with 1σ confidence band (gray, shaded) are shown, whose intercept can be used to impute $q_{R,\text{magic}} (\text{expt.}) = 0.350(6)$. The analytic expression for the curvature (red) is consistent with the data-driven analysis of the curvature, cf. $q_{R,\text{magic}} (\text{theory}) = 0.348$. The left [right] vertical axis shows the curvature $\partial^2 f_{12}/\partial B_z^2$ [$\Omega \partial^2 \omega_{12}/\partial \Delta^2$] in absolute units of kHz/G² [dimensionless units]. The normalized curvature is unity when $q_R = 0$.

sionless units – with the splitting and detuning normalized to the Rabi frequency – $(\Omega \partial^2 \omega_{12}/\partial \Delta^2)_{\min} = 0.02$, which is 50–fifty times lower than the curvature of this transition for the second-order decoupled ($q_R = 0$) case.

Despite long coherence times, the low duty cycle ($D < 0.01$) and large dead-time-low repetition rate ($T_{\text{shot}} \gtrsim 10$ s) of cold quantum gas experiments make achieving it challenging metrological sensitivities per unit bandwidth that are competitive with other platforms. Here $D = 0.005$ and $T_{\text{shot}} = 20$ s, yet we make many more spin projection measurements ($[N_m = \text{blah}]$ at a shot-noise limited SNR of 10–100 [25]) than traditional cold atom experiments ($N_m = 1$ to several, e.g. absorption or dispersive imaging). This intra-shot revelation of the time and frequency domain renders the measurement of these spectra orders of magnitude more efficient. For example, the single spectrum shown in Fig. 3 would take $\sim (10 \text{ shots per } \delta B_z \text{ per } \omega_{ij}) \times (100 \delta B_z \text{ values}) \times (3 \text{ transitions } \omega_{ij}) = 3000 \text{ shots}$, or $\sim 6 \times 10^4 \text{ s} = 1000 \text{ minutes}$ of data acquisition. We acquire this spectrum in a single shot, i.e. 20 s. The data used to generate Fig. 4 was acquired in only 5 minutes.

In summary, we have demonstrated real-time measurement of continuous dynamical decoupling in a spin-1 quantum gas, and expeditious optimization of this de-

coupling by varying the the relative asymmetry of the Zeeman state splittings. Continuous weak measurement via the Faraday effect yields information about the rf-dressed superposition, the dressed-state couplings and energies, simultaneously. In this measurement regime, we do not resolve the quantum noise of the decoupled collective spin. With a modification of the probe (atom-shot noise dominated) we could measure and affect the quantum noise dynamically, and probing the dressed state coherences in this regime may expose non-Gaussian quantum noise geometries in a manner analogous to Ref. [31]. Our time-frequency reduction of the weak measurement record make plain the cyclic coupling of all three dressed states, which could be applied to emulating quantum spin ladders with frustrated interactions. By making the coupling spatially dependent, the optimal decoupling of the synthetic clock states demonstrated can be applied to critical phenomena in spin-orbit coupled spin-1 Bose gases, as $q = q_{R,\text{magic}} \Omega$ traverses the polar-stripped and plane-wave phases in the vicinity of a tricritical point of the (Ω, q) phase diagram [32]. Indeed the Faraday probe beam – used to detect magnetization – could constitute one of the Raman beams used to generate the spin-orbit coupling.

-
- [1] M. J. Biercuk, H. Uys, A. P. VanDevender, N. Shiga, W. M. Itano, and J. J. Bollinger, *Nature* **458**, 996 (2009).
 - [2] G. d. Lange, Z. H. Wang, D. Ristè, V. V. Dobrovitski, and R. Hanson, *Science* **330**, 60 (2010).
 - [3] H. Bluhm, S. Foletti, I. Neder, M. Rudner, D. Mahalu, V. Umansky, and A. Yacoby, *Nature Physics* **7**, 109 (2011).
 - [4] F. F. Fanchini, J. E. M. Hornos, and R. d. J. Napolitano, *Physical Review A* **75**, 022329 (2007).
 - [5] M. Hirose, C. D. Aiello, and P. Cappellaro, *Physical Review A* **86**, 062320 (2012).
 - [6] M. Loretz, T. Rosskopf, and C. L. Degen, *Physical Review Letters* **110**, 017602 (2013).
 - [7] J.-M. Cai, B. Naydenov, R. Pfeiffer, L. P. McGuinness, K. D. Jahnke, F. Jelezko, M. B. Plenio, and A. Retzker, *New Journal of Physics* **14**, 113023 (2012); J. Cai, F. Jelezko, N. Katz, A. Retzker, and M. B. Plenio, *New Journal of Physics* **14**, 093030 (2012).
 - [8] D. A. Golter, T. K. Baldwin, and H. Wang, *Physical Review Letters* **113**, 237601 (2014).
 - [9] N. Aharon, M. Drewsen, and A. Retzker, *Physical Review Letters* **111**, 230507 (2013).
 - [10] P. Facchi and S. Pascazio, *Physical Review Letters* **89**, 080401 (2002); P. Facchi, D. A. Lidar, and S. Pascazio, *Physical Review A* **69**, 032314 (2004).
 - [11] R. Vijay, C. Macklin, D. H. Slichter, S. J. Weber, K. W. Murch, R. Naik, A. N. Korotkov, and I. Siddiqi, *Nature* **490**, 77 (2012).
 - [12] A. Valdés-Curiel, D. Trypogeorgos, E. E. Marshall, and I. B. Spielman, *New Journal of Physics* **19**, 033025 (2017).
 - [13] C. F. Ockeloen, R. Schmied, M. F. Riedel, and

- P. Treutlein, [Physical Review Letters](#) **111**, 143001 (2013); A. Horsley and P. Treutlein, [Applied Physics Letters](#) **108**, 211102 (2016).
- [14] D. M. Stamper-Kurn and M. Ueda, [Reviews of Modern Physics](#) **85**, 1191 (2013).
- [15] H.-J. Mikeska and A. K. Kolezhuk, in *Quantum Magnetism*, Lecture Notes in Physics No. 645, edited by U. Schollwöck, J. Richter, D. J. J. Farnell, and R. F. Bishop (Springer Berlin Heidelberg, 2004) pp. 1–83.
- [16] E. Majorana, *Il Nuovo Cimento* (1924-1942) **9**, 43 (1932).
- [17] J. M. Boss, K. S. Cujia, J. Zopes, and C. L. Degen, [Science](#) **356**, 837 (2017); S. Schmitt, T. Gefen, F. M. Stürner, T. Uden, G. Wolff, C. Müller, J. Scheuer, B. Naydenov, M. Markham, S. Pezzagna, J. Meijer, I. Schwarz, M. Plenio, A. Retzker, L. P. McGuinness, and F. Jelezko, [Science](#) **356**, 832 (2017).
- [18] N. Ramsey, *Molecular beams* (Clarendon Press, 1956).
- [19] F. Gerbier, A. Widera, S. Fölling, O. Mandel, and I. Bloch, [Physical Review A](#) **73**, 041602 (2006).
- [20] G. A. Smith, S. Chaudhury, A. Silberfarb, I. H. Deutsch, and P. S. Jessen, [Physical Review Letters](#) **93**, 163602 (2004).
- [21] The curvature of the dressed-state energies is evaluated using perturbation theory. In particular, the dimensionless curvature of ω_{12} is $\partial^2(\omega_{12}/\Omega)/\partial(\Delta/\Omega)^2 = \Omega \partial^2 \omega_{12}/\partial \Delta^2 = -(3q_R \sqrt{4+q_R^2} - q_R^2 - 2)/(2\sqrt{4+q_R^2})$. For $q_R=0$, we recover the spin-1/2 result, $\Omega \partial^2 \omega_{12}/\partial \Delta^2 = 1$.
- [22] The curvature of the dressed-state energies is evaluated using perturbation theory. In particular, the dimensionless curvature of ω_{12} is $\partial^2(\omega_{12}/\Omega)/\partial(\Delta/\Omega)^2 = \Omega \partial^2 \omega_{12}/\partial \Delta^2 = -(3q_R \sqrt{4+q_R^2} - q_R^2 - 2)/(2\sqrt{4+q_R^2})$. For $q_R = 0$, we recover the spin-1/2 result, $\Omega \partial^2 \omega_{12}/\partial \Delta^2 = 1$.
- [23] We take $\Delta = -\gamma \delta B_z$ for $|\Delta| \leq 2\Omega$ ($|\delta B_z| \leq B_{rf}/2$) and $|\partial q/\partial \Delta| \approx |\gamma^{-1} \partial q/\partial B_z| = |2B_z q_Z/\gamma| \ll 1$, valid to 10^{-3} for the field strengths $B_z \lesssim 5$ G used here, resulting in vanishing third-order derivatives of ω_i with respect to detuning. In general, the variation of q with Δ (or δB_z) can be accounted for using the Breit-Rabi equation, leading to a residual linear and cubic variation of ω_{12} with δB_z , and a small correction to $q_{R,magic}$ in Eq. (1).
- [24] A. A. Wood, L. M. Bennie, A. Duong, M. Jasperse, L. D. Turner, and R. P. Anderson, [Physical Review A](#) **92**, 053604 (2015).
- [25] M. Jasperse, M. J. Kewming, S. N. Fischer, P. Pakkiam, R. P. Anderson, and L. D. Turner, [arXiv:1705.10965](#) (2017).
- [26] Y. Liu, S. Jung, S. E. Maxwell, L. D. Turner, E. Tiesinga, and P. D. Lett, [Physical Review Letters](#) **102**, 125301 (2009); G. A. Smith, A. Silberfarb, I. H. Deutsch, and P. S. Jessen, [Physical Review Letters](#) **97**, 180403 (2006).
- [27] S. Chaudhury, G. A. Smith, K. Schulz, and P. S. Jessen, [Physical Review Letters](#) **96**, 043001 (2006).
- [28] N. Lundblad and I. B. Spielman, [arXiv:1706.xxxxx](#) (2017).
- [29] The experiment is synchronized to the mains power line; the harmonic composition of which varies little between contiguous shots (20 s apart), and thus the measured $\delta B_z(t)$ and $q(t)$ from the calibration [fiducial?] shot serve as a good proxy for the values experienced by the atoms in the subsequent ~~C6DB~~-decoupled shot.
- [30] A. Messiah, *Quantum mechanics*, Vol. 2 (North-Holland, 1962).
- [31] G. Colangelo, F. M. Ciurana, L. C. Bianchet, R. J. Sewell, and M. W. Mitchell, [Nature](#) **543**, 525 (2017).
- [32] G. I. Martone, [Physical Review Letters](#) **117** (2016), 10.1103/PhysRevLett.117.125301.